Kinetic and thermodynamic parameters guiding the localization of regioselectively modified kaolin platelets into a PS/PA6 co-continuous blend

Aurélie Taguet, Belkacem Otazaghine, Marcos Batistella

Kinetic and thermodynamic parameters guiding the localization of regioselectively modified kaolin platelets into a PS/PA6 co-continuous blend

Aurélie Taguet [*], Belkacem Otazaghine , Marcos Batistella

Polymers Composites and Hybrids (PCH), IMT Mines Ales, Ales, France

A B S T R A C T

This article highlights the role of kinetic and thermodynamic parameters on the localization of modified kaolin platelets into a high interfacial tension co-continuous PS/PA6 blend after extrusion, injection molding and annealing. Three kinds of copolymers were synthesized and grafted on kaolin: poly(styrene-co-(methacryloyloxy)methyl phosphonic acid) copolymer (P(S-co-MAPC$_1$(OH)$_2$)), polystyrene terminated 3-(mercaptopropyl)triethoxysilane, (ETS-PS) and poly (styrene-co-3-methacryloxypropyltrimethoxysilane) copolymer, (P(S-co-MPS)). Those copolymers were distinguished by (1) the nature of their functional groups (phosphonic acid that reacts only with aluminol groups or alkoxysilane that reacts with both silanol and aluminol groups), (2) the amount of functional groups and (3) their molecular weights. After functionalization the kaolin samples (K1, K2 and K3, respectively) were analyzed by FTIR, TGA and Py-GC/MS to evaluate the grafting. It was shown that P(S-co-MAPC$_1$(OH)$_2$) and P(S-co-MPS) copolymers grafted on kaolin led to highly anisotropic K1 and K3 kaolin platelets, respectively. Then, 50/50/5 PS/PA6/K$_i$ samples (i = 0 to 3) were processed as follows: (1) kaolin platelets were dispersed (via solvent cast) into the PS phase. Then, (2) PS + kaolin were melt mixed by microcompounder with PA6, then (3) the PS/PA6/K$_i$ were injection molded into disks and finally (4) they were annealed (via dynamic or quiescent annealing). Thanks to the high shear rate and longtime of mixing during extrusion (microcompounder), all the kaolin platelets (unmodified K, K1, K2 and K3) crossed the interface and were localized in the PA6 phase. All K$_i$ kaolin stayed in the PA6 phase during injection. However, after annealing (quiescent or dynamic), the localization of the nanoplatelets was guided by thermodynamic parameters, and SEM analysis revealed the segregation of K1 and K3 kaolin platelets at the polymers interface, with a high tendency to impede polymer phases coalescence. Hence, modified K1 and K3 kaolin are promising compatibilizing agents for a co-continuous PS/PA6 blend.

1. Introduction

Co-continuous polymer structures are one of the four basic morphologies of polymer blends with matrix-dispersed particle, matrix-fiber and lamellar structures [1]. Co-continuous polymer blends have wide applications, such as electrical conductive plastics [2,3], scaffolds for drug delivery or tissue engineering [4], filters or membrane supports [5]. Co-continuous morphologies are not stable, due to a highly curved interface, leading to coarsening during annealing. The domain of co-continuity in unfilled blends is dictated by different semi-empirical theories that consider not only volume fraction of each phase but also polymer-polymer interfacial tension and viscosity ratio [6]. For example, polymer blends with high interfacial tension, such as PS/PA6 ($\sigma_{PS/PA6} \approx$ 8 mN/m [7]), have a narrower region of full co-continuity than polymer blends with low interfacial tension because their elongated threads break easily [1,8–10]. Compatibilizers are currently added to stabilize polymer co-continuous morphologies regarding coarsening. Compatibilizers may also modify each polymer proportion to reach the co-continuity zone. Compatibilization can be performed by copolymers using non reactive or reactive routes. As a general tendency, non-reactive compatibilization has a high tendency to reduce the co-continuous region. This tendency of narrowing co-continuous zone has also been evidenced for reactive compatibilizer which also induces a shift in the co-continuous range due to the reaction-induced viscosity changes in one or both phases [9,11,12]. The most commonly used copolymers as compatibilizers for the PS/PA6 blend are: diblock poly (styrene-b-ethylene oxide) [13], random copolymer of styrene and 3-isopropenyl-a,a-dimethylbenzene isocyanate (TMI) [14], PS-grafted-PA6 [14–17], and copolymers based on maleic anhydride and styrene [8, 15,18–21]. It must be noted that only copolymers based on maleic anhydride are commercially available.

Another way to compatibilize polymer blends is to selectively disperse (nano)particles to stabilize the blend. In the case of the PS/PA6 blend, different types of nanoparticles (NPs) were incorporated: montmorillonite [22], silica [23–26], TiO$_2$ [27], carbon nanotubes (CNT) [28]. However, it is well known that selectively dispersing micro or

---

nano-particles at the interface of a high interfacial tension blend is hard, especially for NPs with a high aspect ratio [29,30]. Moreover, also due to their high interfacial tension, polystyrene/polyamide 6 blends have a small range of composition for the co-continuous morphology. Hence, adding (nano)particles will help increasing the domain range of co-continuity. Janus silica nanoparticles were already synthesized and added to be selectively dispersed at the interface and to compatibilize a 80/20 PS/PA6 blend [31]. An amount of 10 phr was needed to fully compatibilize the blend. Even if the synthesis described previously only needed two steps [31], the quantity that can be synthesized, even at an industrial scale is limited. Hence, another way to compatibilize PS/PA6 blends, especially co-continuous ones, and by using low rate of compatibilizers, is to functionalize and disperse commercially available particles bearing anisotropic surface chemistry and relatively high aspect ratio. One particle bringing together these two properties is kaolin.

Hence, in this article, it is proposed to add kaolin particles with a higher aspect ratio than micro-silica and at a lower rate than 10 phr. It is proposed to modify their surface chemistry in order to localize those "intermediate aspect ratio" particles at the interface of a co-continuous 50/50 PS/PA6 blend. Moreover, the two opposing external basal planes of the kaolinite platelets consist of an $AlO_2(OH)_4$ octahedral layer and a SiO_4 tetrahedral layer. This natural asymmetric structure involves a difference of reactivity which allows a selective modification of kaolinite with appropriate molecules or polymers [32]. The anisotropic chemical functionalization of kaolin (due to natural asymmetric structure) will allow segregating the platelets at the interface [33]. Three kinds of structures for the grafting agent were tested: a structure bearing several phosphonic acid functions along the polymer chain, a polystyrene structure with only one trialkoxysilane function at the end of the chain and a structure bearing several trialkoxysilane functions along the polymer chain. The localization will be investigated at each step of the processing (after extrusion, after injection and after annealing).

2. Experimental part

2.1. Materials

The amorphous CRISTAL 1340 polystyrene (PS) purchased from Total Petrochemicals (Feluy, Belgium) was reported to have a high molecular weight, a melt flow index (MFI) of 4 g.10 min^{-1} (with 5 kg at 200 °C) and a density of 1.05 g/cm^3. The Aquamid AQL40 polyamide-6 (PA6) supplied by Aquafil Technopolymers (Arco, Italy) was reported to have a melting point temperature of 220 °C (ISO Test Method 3146), a MFI of 160 g.10 min^{-1} (with 5 kg at 275 °C) and a density of 1.14 g/cm^3. Kaolinite (kaolin Paralux) was purchased from Imerys and came from Brazilian deposits. Its specific surface area was 14.2 ± 0.3 m^2 g^{-1}. The average particle length (d_{50}) of kaolinite was estimated around 0.8 μm [34]. The thickness of a kaolin Paralux platelet varies between 30 and 100 nm. Nanoplatelets are difficult to exfoliate and it will be shown later that they form "stacks" of thickness of about 300 nm. Those "stacks" are called below (micro)particles. Hence, thereafter, we will speak about microparticles of kaolin. PA6 and kaolin were dried during 24 h under vacuum at 80 °C before being processed. Styrene, was purchased from Sigma Aldrich, 3-methacryloxypropyltrimethoxysilane (MPS) and 3-(mercaptopropyl)triethoxysilane (ETS) from ABCR, azobisisobutyronitrile (AIBN) from Fluka, and dimethyl(methacryloxy)methyl phosphonate (MAPC$_1$) from Specific Polymers (Castries, France).

2.2. Synthesis of the grafting agents

2.2.1. Synthesis of the poly(styrene-co-(methacryloyloxy)methyl phosphonic acid) copolymer, P(S-co-MAPC$_1$(OH)$_2$)

The synthesis was performed in several steps and was reported in a previous work [35]. The first step consisted in a radical copolymerization of styrene and dimethyl(methacryloyloxy)-methyl phosphonate

(MAPC$_1$) under argon atmosphere. Into a 100 mL flask fitted with a condenser, 15 g (1.4×10^{-1} mol) of styrene, 1.6 g (7.7×10^{-3} mol) of MAPC$_1$, 0.25 g (1.5×10^{-3} mol) of AIBN and 20 g of acetonitrile were introduced. Argon was bubbled through the mixture for 15 min. The mixture was then stirred and heated at 80 °C for 15 h. After reaction, the polymer (P(S-co-MAPC$_1$)) was purified by precipitation in methanol.

The second step consisted of a hydrolysis of the phosphonate groups of the copolymer obtained from the first step. Into a 100 mL two-necked flask equipped with a Dean Stark apparatus, 10 g of copolymer P(S-co-MAPC$_1$) (90/10 mol%) and 40 mL of dichloromethane were introduced under inert atmosphere. The mixture was degassed by bubbling argon for 15 min, stirred and heated at dichloromethane reflux for 1 h (water was eliminated by the Dean Stark apparatus). The mixture was then cooled at room temperature and 2.7 g (1.8×10^{-2} mol) of bromotrimethylsilane was added dropwise. After 15 h, the solvent was partially eliminated under vacuum, before precipitation of the copolymer P(S-co-MAPC$_1$(OH)$_2$) in methanol. A schematic representation of the grafting agent synthesis process is described in Fig. 1a.

2.2.2. Synthesis of ETS-PS

This grafting agent corresponding to polystyrene chains bearing one trialkoxysilane groups was obtained by free radical telomerization of styrene in presence of 3-(mercaptopropyl)triethoxysilane (ETS). Into a 100 mL flask fitted with a condenser, 15 g (1.4×10^{-1} mol) of styrene, 1.37 g (5.7×10^{-3} mol) of ETS, 0.24 g (1.4×10^{-3} mol) of AIBN and 20 g of acetonitrile were introduced. Argon was bubbled through the mixture for 15 min. The mixture was then stirred and heated at 60 °C for 15 h. After reaction, the polymer ETS-PS was purified by precipitation in methanol. A schematic representation of the grafting agent synthesis process is described in Fig. 1b.

2.2.3. Synthesis of poly(styrene-co-3-methacryloxypropyltrimethoxysilane) copolymer, P(S-co-MPS)

This grafting agent was obtained by copolymerization of a styrene/ MPS 95/5 mol.% mixture. Into a 100 mL flask fitted with a condenser, 15 g (1.4×10^{-1} mol) of styrene, 1.88 g (7.6×10^{-3} mol) of MPS, 0.25 g (1.5×10^{-3} mol) of AIBN and 20 g of acetonitrile were introduced. Argon was bubbled through the mixture for 15 min. The mixture was then stirred and heated at 60 °C for 15 h. After reaction, the polymer P(S-co-MPS) was purified by precipitation in methanol. A schematic representation of the grafting agent synthesis process is described in Fig. 1c.

2.3. Kaolinite modification

Kaolinite functionalization was performed with the same procedure for the three grafting agent. Into a 250 mL flask fitted with a condenser, 10 g of kaolinite, 0.5 g of grafting agent and 100 mL of toluene solution were introduced. The mixture was then stirred and heated at solvent reflux for 15 h. The mixture was next centrifuged (speed: 5000 rpm) to eliminate the liquid phase and washed three times with THF. Finally, the obtained kaolinite was dried under vacuum.

2.4. Ternary (micro)composite preparation and annealing

Ternary (micro)composites based on 50 wt% of PS, 50 wt% of PA6 and 5 per hundred rates (phr) of kaolin were prepared. In a first step, pure or modified kaolin microparticles (MPs) were embedded into PS film by a solvent cast method. Details are explained elsewhere [24]. In a second step, kaolin MPs embedded in PS were melt mixed under nitrogen in a mini-extruder DSM (Xplore) with a screw length of 135 mm and a chamber volume of 15 cm^3. The temperature was set at 240 °C and the screw speeds used were 60, 120 and 40 rpm during incorporation (1min), mixing (4min) and extrusion (almost 2 min), respectively. After pelletizing, the granules were dried under vacuum at 80 °C overnight and then injection-molded onto discs (diameter of 25 mm, thickness of 1.5 mm) for rheological analyses using a mini injection-molding
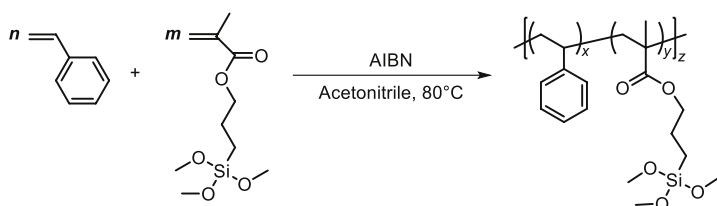
a) Synthesis of P(S-co-MAPC₁(OH)₂)
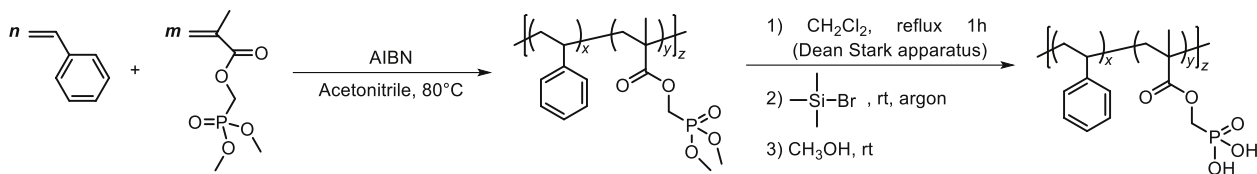
b) Synthesis of ETS-PS
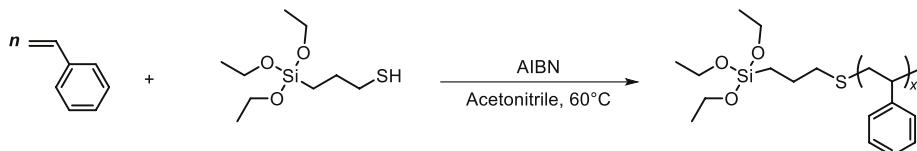
c) Synthesis of P(S-co-MPS)

Fig. 1. Schematic representation of the synthesis of the three polymer grafting agents: (a) P(S-co-MAPC₁(OH)₂), (b) ETS-PS and (c) P(S-co-MPS).

machine (MERCATOR, Zamak). The barrel temperature was set at 240 °C.

Quiescent annealing was performed at 230 °C under nitrogen for 30 min on the thread after mini-extruder. Dynamic annealing was performed on discs under rheological tests (see § 3.5.8).

2.5. Characterization

2.5.1. ¹H NMR
NMR spectra were recorded on Bruker AC 400 instruments, using deuterated chloroform as the solvent and tetramethylsilane as the references for ¹H nuclei. Chemical shifts are given in part per million (ppm). The experimental conditions for recording ¹H NMR spectra were as follows: flip angle 90°, acquisition time 4.5 s, pulse delay 2 s and number of scans 16.

2.5.2. Size exclusion chromatography (SEC)
SEC was performed on a Varian apparatus equipped with a RI Shodex refractive index detector, two PL gel Mix C columns at 35 °C with a 1 mL min⁻¹ flow rate of tetrahydrofuran (THF), and calibrated using polystyrene standards.

2.5.3. TGA
The grafting of kaolinite was studied by thermal gravimetric analysis (TGA). Thermal characterization was carried out with a PerkinElmer Pyris-1 instrument on 10 mg of samples, under nitrogen. Samples were first heated at 10 °C/min from 25 to 110 °C, followed by an isotherm at 110 °C for 10 min to remove all the physisorbed water of the kaolinite. They were then heated again from 110 to 900 °C, at 10 °C/min, in order to eliminate the grafted groups.

2.5.4. Py-GC/MS
A Pyroprobe 5000 pyrolyzer (CDS analytical) was used to flash pyrolyze the samples in a helium environment. This pyrolyzer is supplied with an electrically heated platinum filament. One coil probe enables the pyrolysis of samples (<1 mg) placed in a quartz tube between two pieces of rockwool. The sample was heated at 900 °C. The temperature

was held for 15 s, and then the gases were drawn to the gas chromatograph for 5 min. The pyroprobe 5000 is interfaced to a 450-GC chromatograph (Varian) by means of a chamber heated at 270 °C. In the oven, the initial temperature of 70 °C was raised to 250 °C at 10 °C/min. The column is a Varian Vf-5 ms capillary column (30 m × 0.25 mm; thickness = 0.25 μm) and helium (1 l/min) was used as carrier gas, a split ratio was set to 1:50. The gases were introduced from the GC transfer line to the ion trap analyzer of the 240-MS mass spectrometer (Varian) through the direct-coupled capillary column.

2.5.5. Contact angle measurement
Contact angle measurements were carried out by depositing a liquid drop with controlled volume on the sample surface. The contact angle θ between the liquid and the substrate was measured using a KRÜSS Drop Shape Analyzer DSA30 goniometer apparatus. Thin flat disks of kaolin were prepared using a compression molded laboratory press. Then, contact angle measurements between sample surface and water were performed ten times.

2.5.6. Solvents dispersion test
A dispersion test in a water/toluene mixture was also completed on kaolinites before and after modification. 5 mg of clay was introduced in 2 mL of water and ultrasonically dispersed for 5 min. 2 mL of toluene was then added and the whole was mixed ultrasonically for another 5 min. The mixtures were left for 1 week and pictures were taken at different times.

2.5.7. Morphology characterization
Scanning Electron Microscope (SEM) was used to evaluate the morphology of the ternary microcomposites and especially the localization of pure and modified kaolin, before and after annealing. An environmental SEM Quanta 200 FEG (FEI Company) was operated under high vacuum at 10 kV. All the samples were prepared by cryofracture and coated with a thin carbon layer. Before annealing, the images were collected either on threads after melt mixing or on discs samples after injection molding. After annealing, the images were collected either after heating (quiescent annealing) or after rheological

test (dynamic annealing), as mentioned previously. For some micrographs, one of the two co-continuous phases was extracted in an appropriate solvent: PA6 and PS were dissolved in formic acid and THF, respectively.

2.5.8. Rheological tests

Oscillatory shear measurements were performed using an advanced rheometric expansion system (ARES, TA Instruments). All the tests were carried out under nitrogen atmosphere on sample discs, which were dried under vacuum at 80 °C for 24 h. The measurements were performed at 240 °C using the plate–plate geometry. The plate diameter was 25 mm and the gap between the two plates was set to 1 mm. A shear strain of 3% was chosen for all subsequent frequency sweep tests. The frequency was varied from 100 to 0.1 rad s^{-1}. Discs were collected after rheological tests to evaluate the evolution of their microstructure after dynamic annealing.

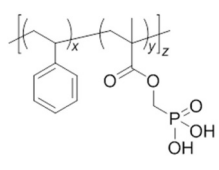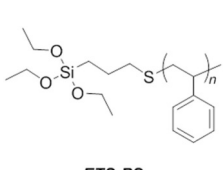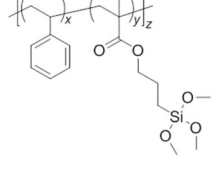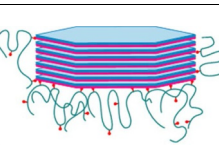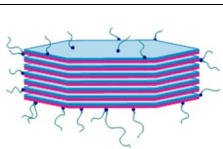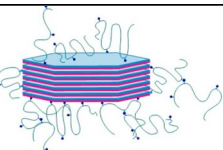## 3. Results

3.1. Synthesis of the copolymers

It is well known that kaolin platelets as all the silicates will prefer to localize in PA6 when melt mixed into a PS/PA6 blend. Hence, to improve affinity with the PS phase in the PS/PA6 blend, kaolinite surface was functionalized with copolymers bearing PS chains. So, in a first step of this article, we have developed synthesis procedures to obtain polystyrene chains bearing chemical functional groups: alkoxysilane and phosphonic acid groups, allowing the formation of a covalent bond with functional groups at the kaolinite surface. Kaolin exhibits an asymmetric surface chemistry that can lead to dual modification showing interfacial activity in immiscible blends such as in solvent-cast PS/PMMA blend film [32]. Indeed the structure of kaolinite contains aluminosilicate layers comprised of a tetrahedral SiO_4 sheet and an octahedral AlO_6 sheet. The alumina surface is covered with Al–OH groups, whereas the silica surface is mainly composed of siloxane Si–O–Si groups. Nevertheless, some Si–OH hydroxyl groups are present at the silica surface. Al–OH or Si–OH groups are also present on the edges and in defects of the aluminosilicate layers. Because hydroxyl groups are rare at the silica surface and edge, the kaolinite surface chemical reactivity is predominantly related to that of Al–OH groups at the alumina surfaces. Hence, we assume that the grafting of kaolinite with alkoxysilane grafting agents will give heterogeneity of surface functionalization. Moreover, the grafting of kaolinite with phosphonic acid groups (which are known to react only with aluminol groups) will also lead to asymmetric surface functionalization.

PS based copolymer grafting agents were synthesized by radical polymerization to obtain polymer chains bearing phosphonic acid or alkoxysilane groups. The structures of the different grafting agents are represented in Table 1. Phosphonic acid functions are known to react only with aluminols [35] and the copolymer P(S-co-MAPC$_1$(OH)$_2$) was synthesized for the selective modification of alumina faces. Its synthesis and characterization were described in a previous work about selective modification of halloysite [35]. PS chains bearing alkoxysilanes functions were used to modify silica and alumina faces of kaolinite particles because these functions are reactive with silanols and aluminols [36]. Two kinds of structure where obtained for the PS chains bearing alkoxysilane groups: a structure with only one trialkoxysilane function at the end of the chain (ETS-PS) and a structure bearing several trialkoxysilane functions along the polymer chain (P(S-co-MPS)). ETS-PS was obtained by radical telomerization of styrene in presence of ETS as transfer agent. P(S-co-MPS) was obtained by radical copolymerization of styrene with MPS.

These grafting agents were characterized by ^{1}H NMR to validate their structure and by Size-Exclusion Chromatography (SEC). Fig. 2 shows the

Table 1

Characteristics of the PS based grafting agents and schematic representations of the obtained kaolinite platelets functionalization.

Grafting agent	P(S-co-MAPC$_1$(OH)$_2$)	ETS-PS	P(S-co-MPS)
M_n (I_p) [a] (g/mol.)	4600 (1.8)	2800 (4.7) (5300 from NMR analysis)	10100 (2.4)
x_g [b] (mol%)	5.4	-	6.3
Functionalization	K1	K2	K3
Schematic representation			
Grafting rate [c] (wt%)	2.0	1.3	2.1
Molar grafting rate (mol./g) [d]	4.3×10^{-6}	4.6×10^{-6}	2.1×10^{-6}

[a] values obtained from SEC analyses.
[b] x_g corresponds to the molar fraction of the monomer units bearing the grafting group and was calculated from NMR ^{1}H analyses.
[c] values calculated from TGA.
[d] values calculated from TGA and SEC results.

NMR spectra of the three synthesized grafting agents. The NMR spectrum of ETS-PS (Fig. 2b) shows a large signal centered at 3.8 ppm corresponding to the protons of the methylene group in α-position of the oxygen of the ethoxysilane groups. A comparison between the intensity of this signal characteristic of the alkoxysilane end chains and the intensity of the signal centered at 6.9 ppm characteristic of the aromatic protons of styrene units allows to determine a molecular weight (M_n) of about 5300 g/mol whereas the SEC analysis of this sample gives M_n of about 2800 g/mol. This difference is due to an incomplete functionalization of the PS chains obtained by the radical telomerization. Indeed only one part of the obtained polymer chains bears an ethoxysilane group. Hydrolysis of one part of the ethoxysilane functions could also explain the difference between the NMR and SEC analyses. However, this explanation is unlikely due to the stability of these functions and the use of anhydrous conditions for the preparation of this grafting agent.

The NMR spectrum of P(S-co-MPS) (Fig. 2c) shows a large signal centered at 3.6 ppm corresponding to the protons of the methyl groups of the alkoxysilane functions carried by MPS units. This signal also exhibits a peak corresponding to the protons of the methylene group in α-position of the oxygen of the ester functions. A comparison between the intensity of this signal characteristic of MPS units and the intensity of the signal centered at 6.9 ppm characteristic of the aromatic protons of styrene units gives a molar percentage of about 6.3 for the MPS units. For this grafting agent, the SEC analysis gives a molar weight of about 10100 g/mol. The calculation from these NMR and SEC results gives polymer chains of about 89 units with about 5–6 silane units per chain.
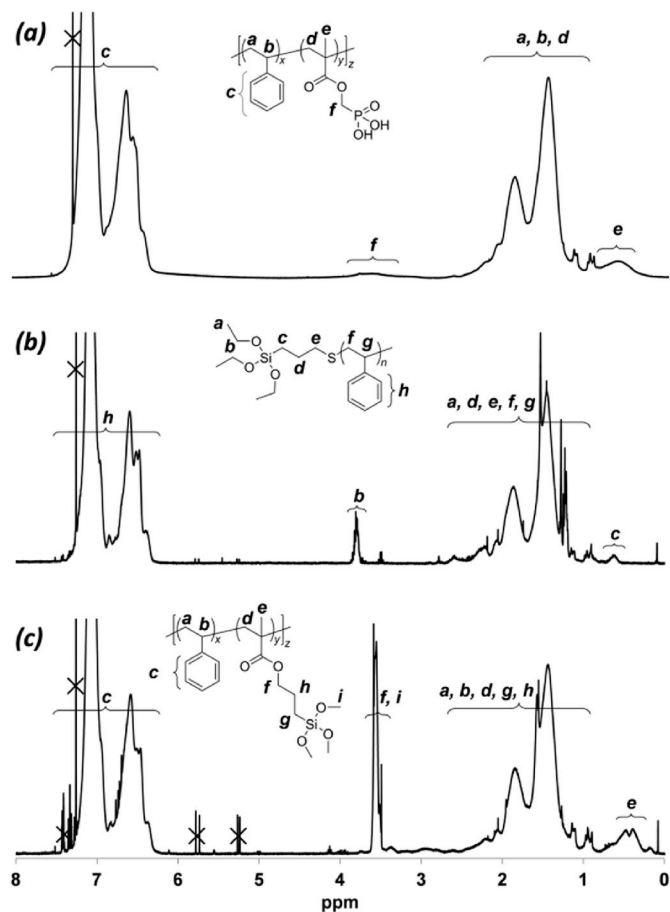
3.2. Kaolinite grafting with PS based copolymers

Kaolinite was functionalized by the three PS based grafting agent using the same procedure. The modification was performed with a filler/grafting agent rate equal to 100/5 (weight equivalent). Py-GC/MS was used to characterize the modification of kaolinite. Total ion chromatograms (TIC) of kaolinite modified with P(S-co-MAPC$_1$(OH)$_2$) (noted K1), with ETS-PS (noted K2) and with P(S-co-MPS) (noted K3) predominantly show the formation of styrene after pyrolysis due to the degradation of the PS chains (Fig. 3a, b and c). These results confirm the presence of the grafting agent after surface modification of kaolinite. Moreover, the extracted ion chromatograms (EIC) at m/z 86 of K1 and K3 (Fig. 3d and e) show the presence at 3.7 min of a peak characteristic of methacrylic acid. The presence of this compound is due to the decomposition during the pyrolysis step of the methacrylate units of the polymer grafting agents: MAPC$_1$(OH)$_2$ for K1 and MPS for K3.

TGA was then used to quantify the grafting rate (Fig. 4). As mentioned previously, P(S-co-MAPC$_1$(OH)$_2$) is expected to react only with the aluminol groups whereas ETS-PS and P(S-co-MPS) are expected to react on both silanol and aluminol groups [37]. Moreover, it is known that the alumina surface bears more free hydroxyl groups than the silica one. The grafting rates obtained for the modification of K1, K2 and K3 kaolinite are about 2.0, 1.3 and 2.1 wt% respectively. These rates correspond to grafting efficiencies of about 42, 27 and 44% for P(S-co-MAPC$_1$(OH)$_2$), ETS-PS and P(S-co-MPS), respectively.

A molar grafting rate for the modified kaolinite samples was obtained by the comparison of the TGA results and the M_n values obtained by SEC for the three grafting agents. Rate values of about 4.3×10^{-6}, 4.6×10^{-6} and 2.1×10^{-6} mol/g were calculated for K1, K2 and K3,

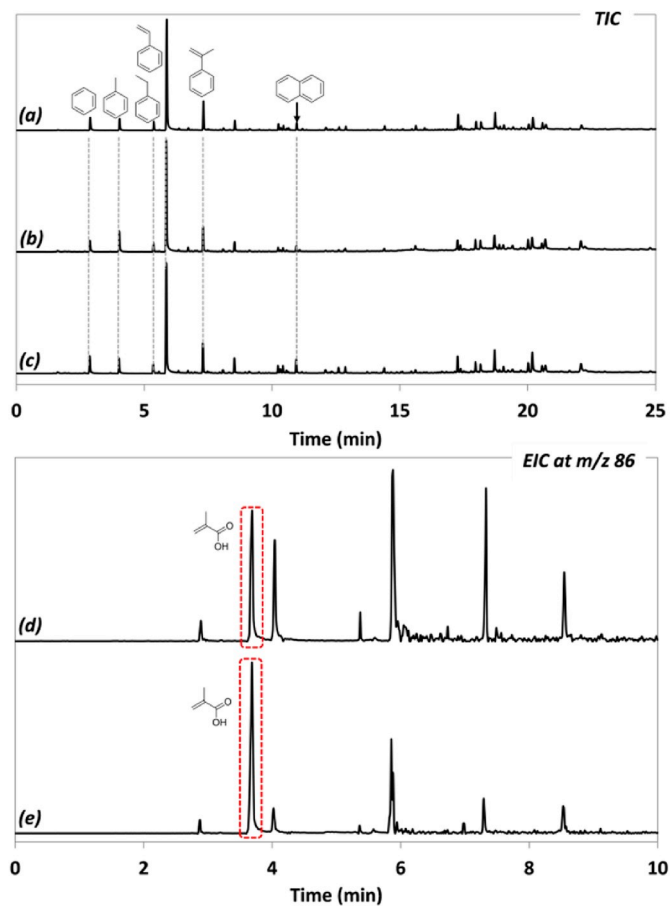

Fig. 2. ^{1}H NMR spectra of synthesized grafting agents: (a) P(S-co-MAPC1 (OH)$_2$), (b) ETS-PS and (c) P(S-co-MPS).

Fig. 3. Py-GC/MS TIC of modified kaolinite samples (a) K1, (b) K2, (c) K3 and EIC at m/z 86 of (d) K1 and (e) K3.
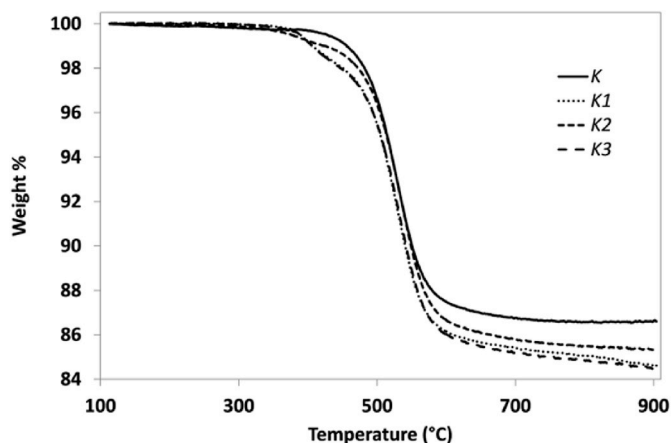
Fig. 4. TGA under nitrogen, from 110 °C to 900 °C and after an isotherm at 110 °C for 10 min, of pristine and modified kaolinite.

respectively (Table 1). So the less molar grafting rate was obtained with the grafting agent having the highest M_n value and bearing the most grafting functions by chains.

To evaluate the effect of the grafting on the free surface energy of kaolinite, contact angle measurements were carried out by putting water drops on the surface of flat discs of kaolinite obtained by compression molding of the clay powder. For pristine kaolinite and K2 the water drop is instantly absorbed and no measurement can be done. Whereas for K1 and K3 the water drop is not absorbed by the kaolinite disc and contact angles of about 95 ± 4° and 104 ± 3°, respectively can be measured (Table S1). This modification of affinity proves the presence of chains with low polarity on the platelet surfaces for K1 and K3. We assume that the high affinity with water for K2 is due to an insufficient coverage of the kaolinite surface by the PS grafting agent. We assume that the difference of structure for the three PS grafting agents must involve differences of surface coverage. Indeed chains bearing several grafting functions (allowing the formation of a covalent bond with the kaolinite surface), such as for K1 and K3, combined with high molecular weights must allow a high coverage of the surface with polymer forming brushes. Whereas, chains bearing only one grafting function at the chain end and having a low molecular weight (this is the case of K2) must lead to a low coverage of the kaolinite surface. A schematic representation of the final grafting morphology is shown in Table 1.

The unmodified (K) and the three modified (K1, K2 and K3) kaolins were dispersed in an immiscible toluene/water mixture to evaluate their capacity to stabilize a water-oil Pickering emulsion. Fig. 5 clearly establishes that all modified kaolins promote the long-term stability of the Pickering emulsion, whereas the unmodified kaolin K do not stabilize the W/O emulsion.

The shape and size of the water droplets in the toluene media are very different depending on the kaolin functionalization (Fig. 6). P(S-co-MAPC$_1$(OH)$_2$) grafted kaolin platelets (K1) exhibit the best emulsification capability (Fig. 6b). K1 leads to the finest water droplets, probably due to the regioselective grafting on aluminol groups leading to a perfectly anisotropic NP. Then, P(S-co-MPS) grafted kaolin platelets (K3) lead to a stable emulsion with larger droplet size (Fig. 6d). This copolymer exhibits a high molecular weight but not a fully anisotropic grafting on kaolin as it reacts with both silanols and aluminols of the platelets. Finally, ETP-PS grafted kaolin platelets (K2) allow to stabilize the emulsion but the water droplets are very heterogeneous with different shapes and sizes (Fig. 6c). This highlights the poor emulsification capability of the K2 kaolin.
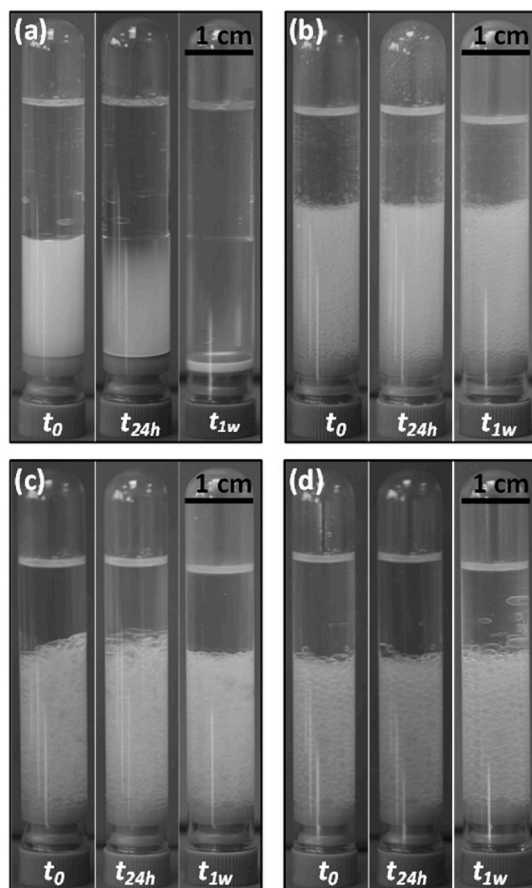

Fig. 5. Dispersion stability of pristine and grafted kaolinites in water–toluene mixture. Images were saved at initial time (after stirring), after 24 h and one week: (a) K; (b) K1; (c) K2; (d) K3.

3.3. Morphology and rheological behavior of ternary microcomposites before annealing

The unfilled PS/PA6 blend exhibits a high interfacial tension leading to a low co-continuous zone that is ranged between 40 and 50 wt% of PS in the blend. The blend is then expected to be co-continuous for the 50/50 PS/PA6 composition. The rheological behavior of the co-continuous blend is classical (Fig. 7). Indeed, G' of the co-continuous blend exceeds that of the two components at low frequency. This increase can be attributed to a longer shape relaxation due to a large interface between PS and PA6 [38].

The viscosity ratio p ($p = \frac{\eta_{PA6}}{\eta_{PS}}$) is relatively close to 2 all along the frequency sweep range (Fig. 7). Then, the migration of NPs from one phase to the other is a priori not limited by the viscosity. This fact is important to be discussed, because as demonstrated by Plattier et al. [39], viscosity of the polymeric phases plays a crucial role in the final localization of the particles. The particles will have a high tendency to stay in the most viscous phase.

The unmodified kaolin (K) is expected to localize in the PA6 phase. Indeed the wetting parameter was estimated based on a surface energy of 171.0, 31.9 and 41.2 mJ/m^2 for kaolin [40], PS and PA6 [24], respectively. Interfacial tension between polymers was calculated using the harmonic mean equation of Wu, whereas interfacial tension between polymers and kaolin was calculated using the geometric mean equation of Owens-Wendt. Hence, for unmodified kaolin in PS/PA6 blend, the wetting parameter is calculated, $\omega_{AB} = 2.7$ (with A = PA6 and B═PS). To predict the localization of each modified kaolin, the use of the wetting parameter is inappropriate. The wetting parameter, ω_{AB} is defined as a mathematical description of the thermodynamic tendency based on the
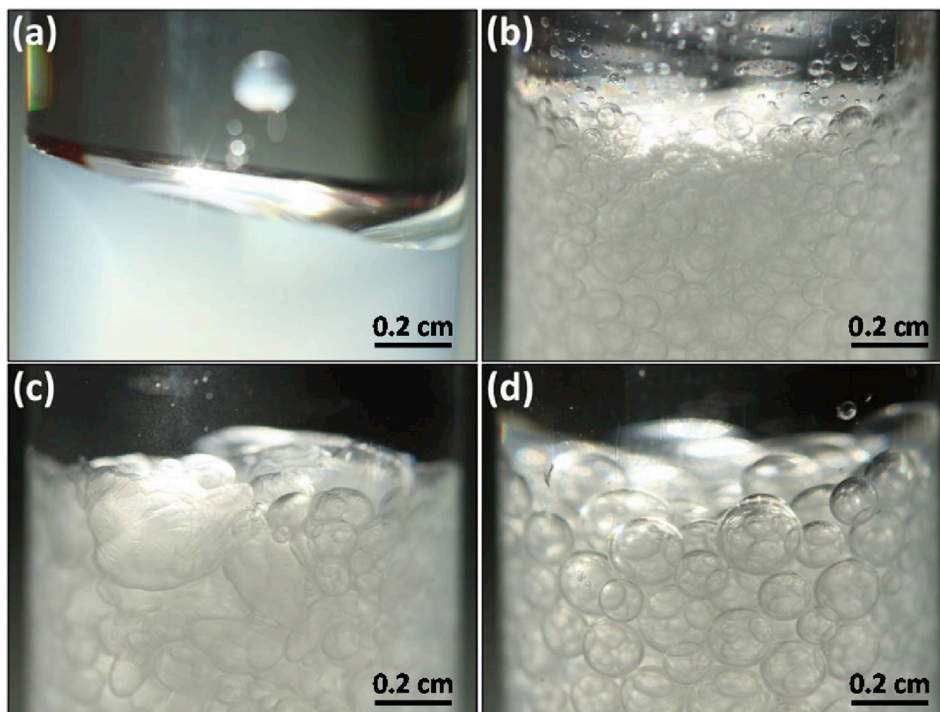
Fig. 6. Dispersion stability of pristine and grafted kaolinites in water–toluene mixture. Images were saved at initial time (after stirring): (a) K; (b) K1; (c) K2; (d) K3.
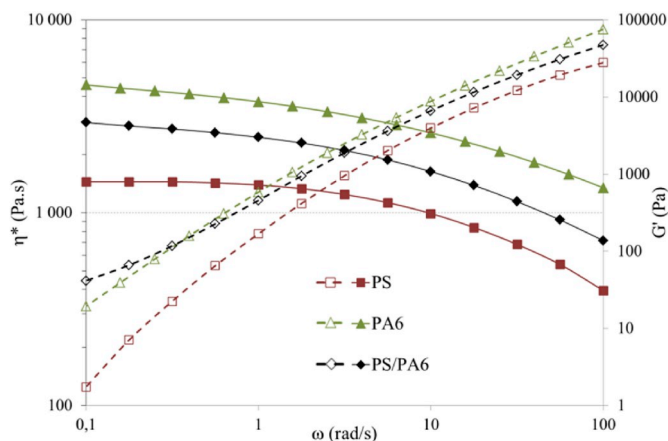

Fig. 7. Complex viscosity and storage dynamic modulus *versus* frequency for PS, PA6 and 50/50 PS/PA6 blend.

measurement of surface tension and the calculation of interfacial tension. However, measuring the surface tension of an asymmetric particle is unfair due to its anisotropic surface chemistry. Moreover, even if the calculation of ω_{AB} predicts the localization at the interface, it is clearly explained by Göldel et al. [41], that in the case of non-spherical NPs, their localization at the interface is an instable transition state and is highly improbable in the final blend morphology. This is particularly pronounced in the case of high aspect ratio NPs (nanotubes) for which only NPs oriented completely parallel to the interface may be stacked at the interface. According to Göldel's "slim-fast mechanism" [42], kaolin platelets can be classified in intermediate transfer speed/interfacial stability. This means that the transfer of kaolin from the PS phase to the PA6 one is not fast but not as low as that of spherical NPs (silica). Hence, to conclude on those previous considerations, unmodified kaolin K is expected to localize in the PA6 phase.

Micrographs of the four formulations (PS/PA6/K to PS/PA6/K3) after extrusion melt mixing and after injection molding are given in the top and in the bottom line of Fig. 8, respectively. It must be noticed that the micrographs of the threads after extrusion (top images in Fig. 8) were performed after selective extraction of PA6 revealing only the PS phase. In all images, kaolin platelets are well-dispersed in the co-continuous blend. Whatever the functionalization, in the threads, there are no platelets in the remaining PS phase (Fig. 8, top). The platelets are dispersed in the dissolved PA6 phase, suggesting that during the extrusion processing platelets migrate from the PS to the PA6 phase, crossing the interface. Then, platelets stay in the PA6 phase during the injection processing as all the platelets are dispersed in this PA6 phase in the images at the bottom of Fig. 8. This implies that, whatever the functionalization, injection does not perform any displacement of the kaolin platelets from the PA6 phase. It is probably due to the short time of mixing applied on the melted blend under mini-injection molding. Another important parameter that plays a crucial role in the localization of NPs is the viscosity of each polymeric phase [39]. In the present case, as the viscosity of PA6 is higher than that of PS (whatever the frequency or shear rate as shown in Fig. 7), it is clear that platelets will have a high tendency to leave the less preferred PS phase and reach the most preferred PA6 phase.

The dynamic viscosity of ternary microcomposites gives interesting information on the morphology of the system and especially dispersion of the microcomposites. PS/PA6/K and PS/PA6/K2 exhibit the same trend (Fig. 9) that is similar to that of the pure blend with a slight increase in viscosity at high and low frequencies. The rheological behavior of PS/PA6/K1 and PS/PA6/K3 is highly different from that of PS/PA6/K and PS/PA6/K2 as seen in Fig. 9. Indeed, those two ternary microcomposites exhibit pseudo-solid-like behavior that is characterized by a G' plateau at low frequency. This is usually attributed to the formation of a percolated particle network of filled particles [43–45].

Fig. 10 shows the microstructure performed on the disks samples after this rheological test. Both final microstructures of PS/PA6/K and PS/PA6/K2 are identical: after the rheological test most of the kaolin platelets are localized in the PA6 phase. On the contrary, at the end of the rheological test, microstructures of PS/PA6/K1 and PS/PA6/K3 clearly showed a localization of the platelets at the interface between PS and PA6 phases (Fig. 10). Hence, the solid network formation at 5 phr of
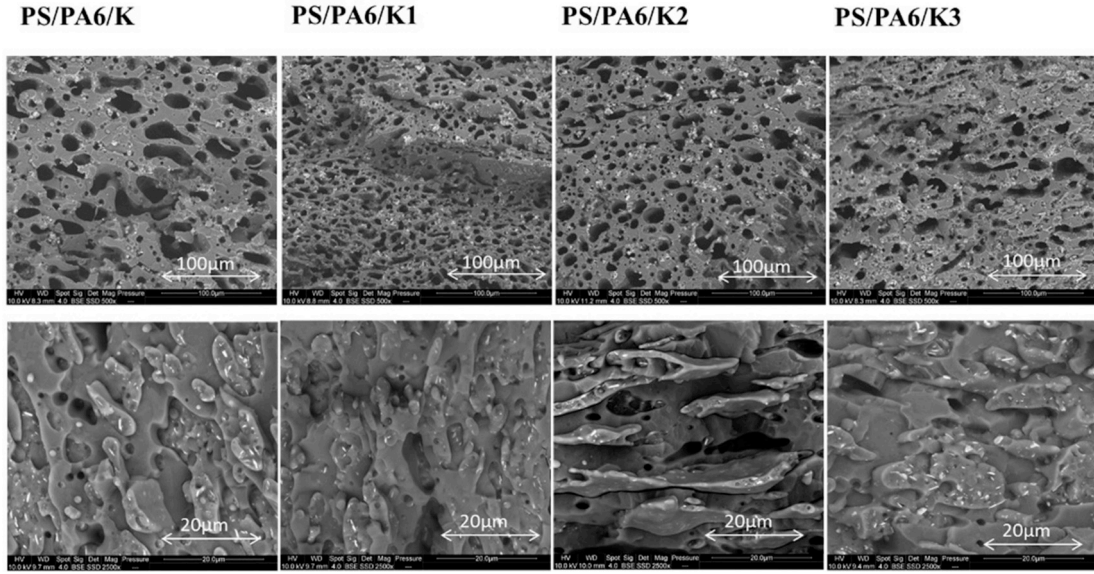
Fig. 8. Micrographs of the thread after extrusion and selective extraction of PA6 by formic acid (top) and of transverse section of discs obtained by mini-injection molding (bottom).
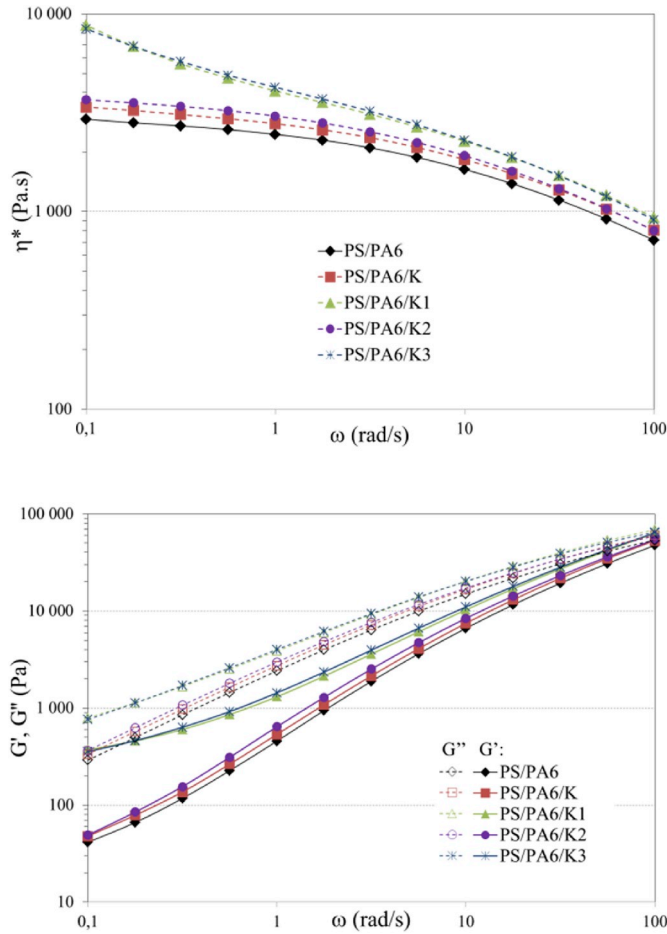
Fig. 9. Rheological measurements (Strain = 3.0%, Temperature = 240 °C, Diameter = 25 mm, Gap = 1 mm).

K1 and K3 functionalized kaolin is due to both the co-continuity of the two polymer phases and the localization of the kaolin at the interface. This peculiar microstructure of both co-continuous polymer phases and

dispersion of NPs at the interface is called the double percolation morphology [46–48]. In our case, it is formed during the rheological test. As platelets were localized in the PA6 before the oscillatory rheological test (Fig. 8), these results also reveal that K1 and K3 kaolin platelets migrate during the rheological test from the PA6 phase to the interface. This migration is accompanied by a coarsening phenomenon that will be discussed latter.

3.4. Ternary microcomposite morphology after annealing

Relaxation of polymer phases performed during quiescent or dynamic annealing is greatly affected by the presence of fillers. After dynamic annealing performed under rheological tests, coarsening is huge for PS/PA6/K and PS/PA6/K2 whereas coarsening is more limited for the PS/PA6/K1 and PS/PA6/K3 formulations (Fig. 10). Unfilled co-continuous morphologies are known to be thermodynamically not stable. During annealing, phases coarsen into larger size domains due to coalescence [49]. These transformations are mainly driven by interfacial tension, and to a lesser extent by viscosity ratio. After dynamic annealing, platelets are localized at the interface for PS/PA6/K1 and PS/PA6/K3. Whereas, platelets remain mainly in the PA6 phase for PS/PA6/K and PS/PA6/K2. The shifting of the platelets at the interface during the dynamic annealing experiment limits the coalescence leading to a finer morphology in the case of PS/PA6/K1 and PS/PA6/K3 than in the case of PS/PA6/K and PS/PA6/K2.

Quiescent annealing were performed on threads after extrusion melt mixing (Fig. 11). The micrographs of Fig. 11 were obtained after selective solvent extraction on threads in order to reveal the undissolved polymer phase and to get insight into the affinity of the kaolin with the phases for the different formulations. The microstructures of the threads before annealing are identical to that of the discs obtained after injection (Fig. 8).

Micrographs of PS/PA6/K and PS/PA6/K2 in Fig. 11 reveal the same microstructure than that of Fig. 10 obtained on disks after rheological tests. That is to say, after quiescent or dynamic annealing, the platelets remain in the PA6 phase with high coarsening. Notwithstanding, co-continuous morphologies are maintained for both PS/PA6/K and PS/PA6/K2.

Micrographs of PS/PA6/K1 and PS/PA6/K3 (Fig. 11) after quiescent annealing reveal the presence of kaolinite K1 and K3 particles mainly at the interface between PS and PA6 but also in the PA6 phase (just as in
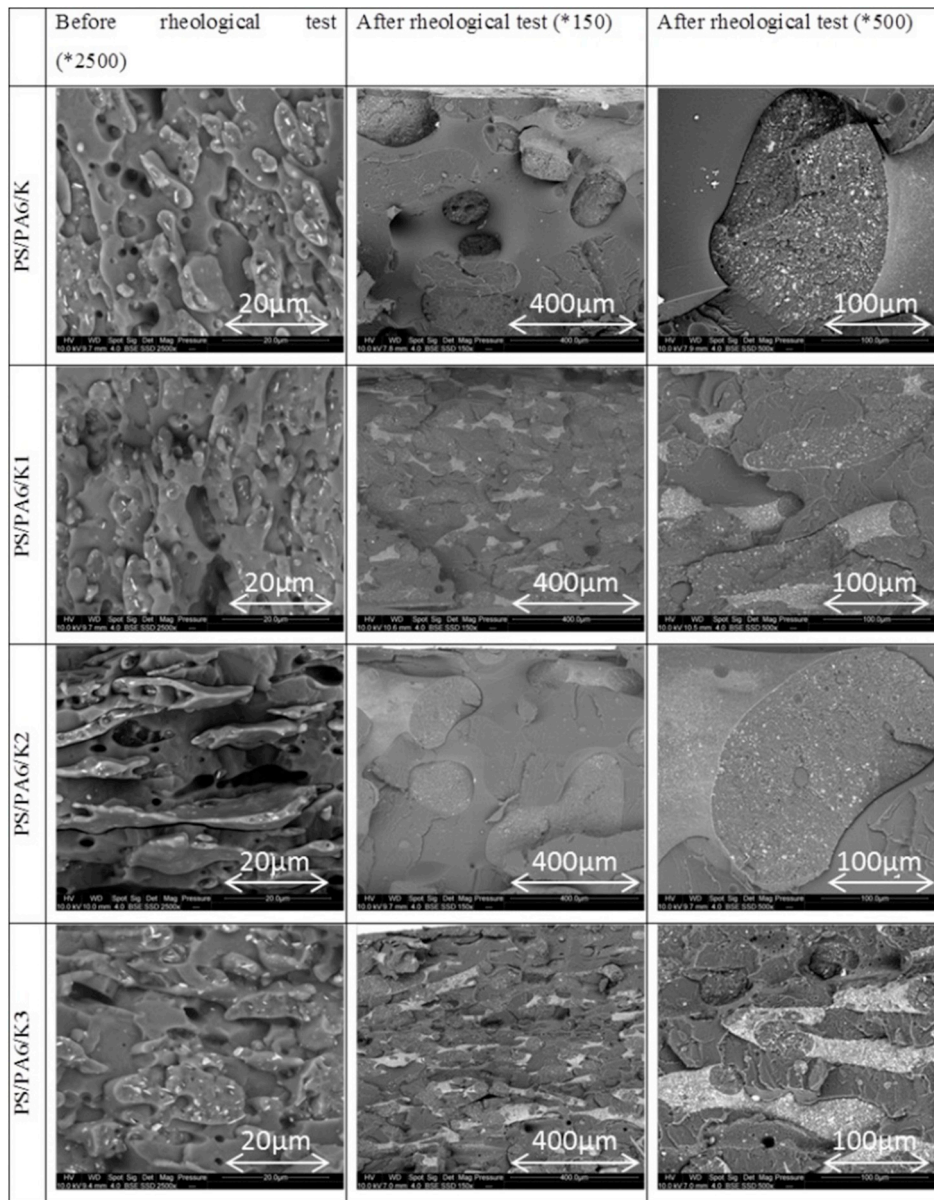
Fig. 10. Micrographs of the disks before (*2500) and after (*150 and *500) rheological test (dynamic annealing).

Fig. 10 after rheological tests). This means that most of the kaolin K1 and K3 platelets migrate during quiescent annealing, from the PA6 phase to the PS/PA6 interface. In order to evidence the localization of the platelets at the interface after annealing in the case of K1 and K3 (contrarily to K and K2), SEM micrographs with high magnification are displayed in Fig. S1. Moreover, the interfacial localization of K1 and K3 after annealing is also supported by SEM/EDX (Fig. S2) that proves the presence of silicon and aluminum elements at the interface of ultra-cryo-microtomed samples collected after rheological tests. As the interface is saturated by the platelets at much smaller amounts than 5 phr (see Fig. S3), it is expected that the remaining K1 and K3 platelets stay in the PA6 phase. Fig. 11 also reveals that interfacially localized K1 platelets have a high affinity with PS as they remain at the surface of the PS phase after the extraction of PA6 with formic acid and they are eliminated when PS is extracted with THF. Contrarily, interfacial K3 platelets have a high affinity with both PA6 and PS as they remain at the surface of both PA6 and PS phases after the extraction of PS and PA6 with THF and formic acid, respectively. This result inquires on the efficiency of the type of functionalization performed on kaolin platelets regarding the

affinity for the polymeric phases.

Moreover, for PS/PA6/K3, the coarsening is less pronounced than for PS/PA6/K1 (see Fig. S4). Indeed, for PS/PA6/K3, coalescence is impeded due to the formation of rigid particle layers at the interface that have a high affinity with both polymeric phases, leading to the decrease or suppression of coarsening.

Xiu et al. [50] defended the formation of a co-continuous structure of 85PLA/15PU/carbon black (CB) with CB high self-networking capability. The formation and stability of co-continuous-like structure was tailored by controlling the self-networking of CB via adjusting relative parameters, such as temperature, shear rate and CB content, indicating a close relation between the self-networking of CB and the formation of co-continuous-like structure. This network cannot be formed during mixing due to the high shear rate that destabilizes the CB network. In this article, the fillers self-networking and stability of fillers network and co-continuous-like structure are created and measured during a rheological test.

In our case, it is evident that the process parameters (shear rate) are not the same for a quiescent or a dynamic annealing than for melt

	PS network BEFORE ANNEALING (PA6 was extracted with formic acid) [1]	PA6 network AFTER quiescent ANNEALING (PS was extracted with THF)	PS network AFTER quiescent ANNEALING (PA6 was extracted with formic acid)
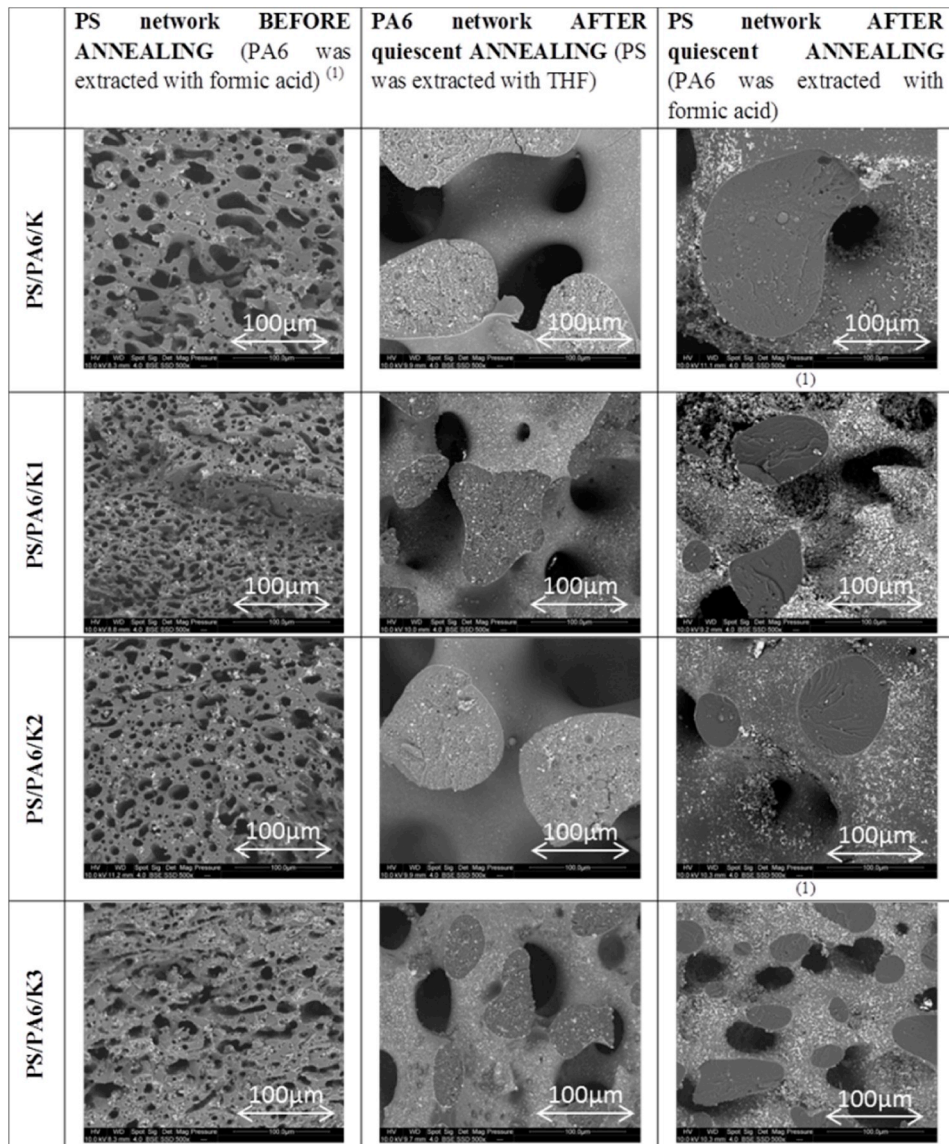
Fig. 11. Microstructures performed on the threads (after extrusion melt mixing) before and after quiescent annealing. First column: PA6 was dissolved in formic acid; second column: PS was dissolved in THF; third column: PA6 was dissolved in formic acid. *(1) The "particles" that can be seen on the surface of the non-extracted phase come from the dissolved phase which has relocated during drying. These particles are then considered as impurities.*

mixing. Then, the migration of the platelets are not governed by the same parameters. During quiescent or dynamic annealing, the final morphologies are guided by thermodynamic parameters (especially, surface chemistry) rather than kinetic parameter. Whereas, during melt mixing, the final localization is guided by the shear rate, time of mixing and intrinsic parameters of the blend (viscosity ratio, interfacial tension, elastic modulus).

When localized at the interface, K3 exhibits a high affinity with both polymer phases. The affinity with the PS phase is due to the PS part of the grafted P(S-co-MPS) copolymer, whereas we assume that the affinity with the PA6 is due to the presence of unreacted silanols groups and Si–O–Si groups of the MPS units of the grafted P(S-co-MPS) copolymer. This leads to a high anisotropic propensity for K3. K3 kaolin is then highly efficient in limiting the coarsening of the co-continuous blend. K1 also localizes at the interface after annealing but exhibits a higher affinity with the PS phase than PA6 phase. Indeed, no P(S-co-MAP-$C_1(OH)_2$) copolymers are grafted on the silanol groups of the silica site of the platelets. K1 limits the coarsening but this impediment effect is more limited than for K3.

4. Discussion

Generally speaking, functionalized kaolins are added in an incompatible co-continuous PS/PA6 blend in order to stabilize the co-continuity and improve the compatibility between the two phases (not shown here). This can only be achieved if the functionalized kaolins localize at the interface. As seen in the previously obtained results, processing route and parameters play a crucial role on the final localization of kaolin platelets. The objective is now to understand the different microstructures of the PS/PA6 blends filled with raw and functionalized kaolinites based on the previous results and regarding the literature.

Pötschke et al. [42] studied the mechanism of transfer through the blend interface during the process for unmodified nanoparticles (carbon black and CNT) that were introduced in the less favorable phase (SAN) to reach the more favorable one (PC). When a solid particle crosses the blend interface during melt mixing, the relaxation of the interfacial curvature has to be considered. Indeed, to achieve a more stable configuration, the interface relaxes by decreasing the curvature to some degree, which drives the wetted particle a certain distance into the more

favorable wetting phase. In the case of spherical NPs (low aspect ratio), this interfacial relaxation can be performed with a small shift of the NP leading to a slow speed transfer and a high interfacial stability. On the contrary, in the case of CNT, if the tube is perpendicular to the interface, interfacial relaxation needs a quasi-full transfer of the nanotube through the interface leading to a fast transfer and a poor interfacial stability. Elongated nanoparticles (nanotubes and platelets) being parallel to the interface are stable because they reduce the system's free energy. This effect of interfacial free energy minimization is high for platelets that exhibit a two-dimensional shape but lower for nanotubes that exhibit only one-dimensional shape. They added that the case of platelets shape nanoparticles is special due to their high probability of parallel orientation to the blend interface. Then, they can reveal high interfacial stability specifically for highly incompatible blend phases.

It must be noticed that the interfacial tension between PC and SAN is very low ($\gamma_{PC/SAN} \approx 0.02\,\mathrm{mJ\,m^{-2}}$) [41] and the blend is a co-continuous PC/SAN one. It is supposed that those previously mentioned conclusions can be extended to submicronic platelets particles such as kaolins.

In low interfacial tension polymer blends, it was shown by Favis et al. that NPs (silica and Cu nanowires) have a high tendency to segregate at the interface [51] because the migration to the interface to further reach the more preferred polymer phase is low. Hence, the process parameters (time of mixing, shear rate) have a high influence on the final morphology, especially for high aspect ratio NPs [30]. They explained that as low interfacial tension have a wide interfacial region, solid particles are blocked at the interface, whereas for high interfacial tension blends, as the region is thin, particles are easily transferred to the preferred phase [52]. In high interfacial tension blends, the NPs do not segregate at the interface. They preferentially reach the most preferred polymer phase because the migration through the interface occurs readily thanks to the thin interfacial region. This phenomenon is particularly evident for low aspect ratio NPs. In the case of high aspect ratio nano-objects, the transfer is slown down and mixing time and shear rates have a great influence on their migration. In the case of micro-scale silica dispersed in high interfacial tension blends, there final localization is mainly influenced by the viscosity of the polymer phases [29]. Hence, an innovative route to segregate MPs and NPs at the interface of a high interfacial tension blend is the use of Janus particles [53–55].

The different morphologies of our high interfacial tension blend filled with modified and unmodified platelets shape particles can now be explained in the light of the above mentioned articles. During the process, whatever the functionalization, the kaolin particles are transferred easily from the PS to the PA6 phase. This transfer is allowed by different parameters: (i) a high interfacial tension between PS and PA6 which leads to a thin interfacial region that allows a high transfer speed to the PA6 phase; (ii) a medium aspect ratio of the NPs which allows a speeder transfer through the interface than for low aspect ratio NPs (such as silica) and (iii) a long mixing time which enhances the above mentioned phenomenon.

However, thermodynamically, regioselectively grafted K1 and K3 platelets exhibit a high tendency to reach the interface. Hence, during the dynamic or quiescent annealing, they migrate from the PA6 phase to the interface thanks to the quiescent conditions of both annealing and the long experimental times. Phenomenon guiding particles motion at the interface of a polymer blend at the melted state are not well understood. There are recent articles dealing with this point. A recent book chapter [56] explains that the migration of particles under dynamic conditions are mainly governed by the frequency of collisions between particles and dispersed phase droplets. These collisions depend on the shear rate and time of mixing. Recently, Jaensson et al. [57] used the Cahn− Hilliard diffuse-interface model to investigate the motion of a rigid particles suspended in two-phase shear flow with one viscoelastic and one Newtonian fluids. By varying the Weissenberg and capillary numbers they proved that four scenarios are possible for the particle: the particle migrates away from the interface; it migrates toward the interface, but its migration is halted; it penetrates the interface into the

Newtonian fluid; or it migrates toward the interface and is adsorbed at the interface. These results obtained by models are promising to understand more about the phenomenon guiding the kaolin particles for K1 and K3 to the interface during annealing but more investigation are needed.

5. Conclusions

High interfacial tension polymer blends, such as PS/PA6 blends are known to impede nano- and microparticles to reach their interface. Kaolin platelets are functionalized with PS bearing copolymers in order to orientate their localization at the interface of a co-continuous PS/PA6 blend. Whatever the functionalization, the extrusion processing (by microcompounder) of the co-continuous PS/PA6/kaolin ternary nanocomposites does not allow to localize the platelets at the interface, even for K1 and K3 NPs. This rapid transfer across the interface during the melt mixing is due to the high interfacial tension of the polymer blend, the relatively high aspect ratio of the NPs, the high shear rate and the long mixing time applied during extrusion. The injection step does not change the morphology and whatever the functionalization, the kaolin stays in the PA6 phase. However, quiescent and dynamic annealing performed after extrusion and injection both allow reaching the most thermodynamically stable microstructures:

- PA6/PS/K and PA6/PS/K2: as the surface recovery density of kaolin platelets with ETS-PS copolymer is low, the K2 modified kaolin platelets are expected to have a chemical behavior close to that of the pure kaolin K. Then, K and K2 remain in the PA6 phase.
- PA6/PS/K1: K1 is modified with $P(S\text{-}co\text{-}MAPC_1(OH)_2)$ copolymer that regioselectively reacted only with the aluminol groups. Hence K1 functionalized platelets exhibit a great affinity with both PS (due to the styrenic part of the grafted copolymer) and PA6 (due to the intrinsic polar behavior of the pure kaolin platelets). Then, this leads to an anisotropic chemical behavior for K1 that segregates at the interface under thermodynamic conditions (during annealing).
- PA6/PS/K3: The grafting of P(S-co-MPS) copolymer onto K3 platelets is highly anisotropic due to the lower density of hydroxyl groups in the silica sites than in the alumina ones. This leads to a much higher grafting rate of P(S-co-MPS) in the alumina sites than in the silica. Moreover, we assume that grafted P(S-co-MPS) chains allow good affinity with PS due to their styrenic part and with PA6 due to the presence of free unreacted Si–OH groups on the P(S-co-MPS) chains. Then, K3 is expected to segregate at the interface under thermodynamic conditions (annealing). And, this high affinity with both polymer phases can explain the presence of the K3 kaolinite particles at the surface of both polymers after extraction and their high tendency to reduce the coalescence.

Hence, these regioselectively modified kaolin platelets are used as compatibilizers of high interfacial tension PS/PA6 blends. To see further investigations on those ternary (micro)composites we can wonder how to control the time of migration at the interface of the modified kaolin platelets during annealing ?

Declaration of competing interest

The authors declare that they have no known competing financial interests or personal relationships that could have appeared to influence the work reported in this paper.

CRediT authorship contribution statement

Aurélie Taguet: Conceptualization, Methodology, Investigation, Writing - original draft, Writing - review & editing, Supervision, Project administration. **Belkacem Otazaghine:** Conceptualization, Methodology, Investigation, Writing - original draft, Writing - review & editing.

References

[1] P. Pötschke, D.R. Paul, Formation of Co-continuous structures in melt-mixed immiscible polymer blends, J. Macromol. Sci. Polym. Rev. 43 (2003) 87–141, https://doi.org/10.1081/MC-120018022.

[2] E. Cohen, L. Zonder, A. Ophir, S. Kenig, S. McCarthy, C. Barry, J. Mead, Hierarchical structures composed of confined carbon nanotubes in cocontinuous ternary polymer blends, Macromolecules 46 (2013) 1851–1859, https://doi.org/10.1021/ma301903n.

[3] Y. Li, H. Shimizu, Conductive PVDF/PA6/CNTs nanocomposites fabricated by dual formation of cocontinuous and nanodispersion structures, Macromolecules 41 (2008) 5339–5344, https://doi.org/10.1021/ma8006834.

[4] P. Salehi, P. Sarazin, B.D. Favis, Porous devices derived from Co-continuous polymer blends as a route for controlled drug release, Biomacromolecules 9 (2008) 1131–1138, https://doi.org/10.1021/bm7010467.

[5] A.-L. Esquirol, P. Sarazin, N. Virgilio, Tunable porous hydrogels from cocontinuous polymer blends, Macromolecules 47 (2014) 3068–3075, https://doi.org/10.1021/ma402603b.

[6] T.S. Omonov, C. Harrats, P. Moldenaers, G. Groeninckx, Phase continuity detection and phase inversion phenomena in immiscible polypropylene/polystyrene blends with different viscosity ratios, Polymer (Guildf) 48 (2007) 5917–5927, https://doi.org/10.1016/j.polymer.2007.08.012.

[7] A.S. Caro-Bretelle, T. Parpaite, B. Otazaghine, A. Taguet, J.M. Lopez-Cuesta, Viscoelastic properties of polystyrene/polyamide-6 blend compatibilized with silica/polystyrene Janus hybrid nanoparticles, J. Rheol. (N. Y. N. Y). 61 (2017) 305–310, https://doi.org/10.1122/1.4975334.

[8] R. Tol, G. Groeninckx, I. Vinckier, P. Moldenaers, J. Mewis, Phase morphology and stability of co-continuous (PPE/PS)/PA6 and PS/PA6 blends: effect of rheology and reactive compatibilization, Polymer (Guildf) 45 (2004) 2587–2601, https://doi.org/10.1016/j.polymer.2003.12.072.

[9] R.C. Willemse, A. Posthuma de Boer, J. van Dam, A.D. Gotsis, Co-continuous morphologies in polymer blends: a new model, Polymer (Guildf) 39 (1998) 5879–5887, https://doi.org/10.1016/S0032-3861(97)10200-2.

[10] P.a. Bhadane, M.F. Champagne, M.A. Huneault, F. Tofan, B.D. Favis, Continuity development in polymer blends of very low interfacial tension, Polymer (Guildf) 47 (2006) 2760–2771, https://doi.org/10.1016/j.polymer.2006.01.065.

[11] P.V. Van Puyvelde, P. Moldenaers, Rheology and morphology development in immiscible polymer blends, Rheol. Rev. (2005) 101–145, doi:10.1.1.361.7276.

[12] R.C. Willemse, Co-continuous morphologies in polymer blends: stability, Polymer (Guildf) 40 (1999) 2175–2178, https://doi.org/10.1016/S0032-3861(98)00430-3.

[13] T.Y. Guo, M.D. Song, G.J. Hao, B.H. Zhang, Compatibility and mechanical properties of polyamide-6/polystyrene/diblock poly(styrene-b-ethylene oxide) copolymer blends, Eur. Polym. J. 37 (2001) 241–246, https://doi.org/10.1016/S0014-3057(00)00118-X.

[14] C.-L. Zhang, C. Li, L. Wang, L.-F. Feng, T. Lin, Dual effects of compatibilizer on the formation of oriented ribbon-like dispersed phase domains in polystyrene/polyamide 6 blends, Chem. Eng. Sci. 178 (2018) 146–156, https://doi.org/10.1016/j.ces.2017.12.008.

[15] C. Lu, S. Guo, L. Wen, J. Wang, Weld line morphology and strength of polystyrene/polyamide-6/poly(styrene-co-maleic anhydride) blends, Eur. Polym. J. 40 (2004) 2565–2572, https://doi.org/10.1016/j.eurpolymj.2004.06.016.

[16] A. Pei, A. Liu, T. Xie, G. Yang, Effect of in situ synthesized macroactivator on morphology of PA6/PS blends via successive polymerization, J. Appl. Polym. Sci. 105 (2007) 1757–1765, https://doi.org/10.1002/app.25650.

[17] C.-L. Zhang, L.-F. Feng, X.-P. Gu, S. Hoppe, G.-H. Hu, Efficiency of graft copolymers as compatibilizers for immiscible polymer blends, Polymer (Guildf) 48 (2007) 5940–5949, https://doi.org/10.1016/j.polymer.2007.07.042.

[18] R.T. Tol, V.B.F. Mathot, G. Groeninckx, Confined crystallization phenomena in immiscible polymer blends with dispersed micro- and nanometer sized PA6 droplets, part 2: reactively compatibilized PS/PA6 and (PPE/PS)/PA6 blends, Polymer (Guildf) 46 (2005) 383–396, https://doi.org/10.1016/j.polymer.2004.10.070.

[19] F.-P. Tseng, C.-R. Tseng, F.-C. Chang, J.-J. Lin, I.-J. Cheng, Compatibilization of PS and PA6 blends by means of poly(oxyalkylene)amine modified styrene-maleic anhydride copolymer, J. Polym. Res. 12 (2005) 439–447, https://doi.org/10.1007/s10965-004-1875-x.

[20] J.-H. Choi, H.-G. Kim, D.-H. Han, J.-C. Lim, D.-H. Oh, K.-E. Min, Effect of processing conditions on compatibility of nylon 6/polystyrene blend, J. Appl. Polym. Sci. 101 (2006) 1–7, https://doi.org/10.1002/app.22081.

[21] C. Yu, D. Shi, J. Wang, H. Shi, T. Jiang, Y. Yang, G.-H. Hu, R.K.Y. Li, Effect of a dual compatibilizer on the formation of co-continuous morphology of immiscible po'lymer blends, Mater. Des. 107 (2016) 171–177, https://doi.org/10.1016/j.matdes.2016.06.044.

[22] J. Yang, L. Sun, S. Xiang, J. He, L. Gu, M. Zhong, Influence of organoclay and preparation technique on the morphology of Polyamide6/polystyrene/organoclay nanocomposites, J. Appl. Polym. Sci. 110 (2008) 276–282, https://doi.org/10.1002/app.

[23] M. Kong, Y. Huang, Y. Lv, S. Wang, Q. Yang, G. Li, Flow-induced morphological instability in nanosilica-filled polyamide 6/polystyrene blends, Polymer (Guildf) 55 (2014) 4348–4357, https://doi.org/10.1016/j.polymer.2014.05.060.

[24] T. Parpaite, B. Otazaghine, A. Taguet, R. Sonnier, A.S. Caro-Bretelle, J.M. Lopez-Cuesta, Incorporation of modified Stöber silica nanoparticles in polystyrene/polyamide-6 blends: coalescence inhibition and modification of the thermal degradation via controlled dispersion at the interface, Polymer (Guildf) 55 (2014) 2704–2715, https://doi.org/10.1016/j.polymer.2014.04.016.

[25] M. Kong, Y. Huang, Y. Lv, Q. Yang, G. Li, Formation and stability of string phase in polyamide 6/polystyrene blends in confined flow: effects of nanoparticles and blend ratio, AIChE J. 62 (2016) 564–573, https://doi.org/10.1002/aic.15058.

[26] X. Zhang, M. Sun, W. Chen, Synergistic effects of silica nanoparticles and reactive compatibilizer on the compatibilization of polystyrene/polyamide 6 blends, Polym. Eng. Sci. 57 (2017) 1301–1310, https://doi.org/10.1002/pen.24511.

[27] X. Cai, B. Li, Y. Pan, G. Wu, Morphology evolution of immiscible polymer blends as directed by nanoparticle self-agglomeration, Polymer (Guildf) 53 (2012) 259–266, https://doi.org/10.1016/j.polymer.2011.11.032.

[28] A.H.A. Hoseini, M. Arjmand, U. Sundararaj, M. Trifkovic, Tunable electrical conductivity of polystyrene/polyamide-6/carbon nanotube blend nanocomposites via control of morphology and nanofiller localization, Eur. Polym. J. 95 (2017) 418–429, https://doi.org/10.1016/j.eurpolymj.2017.08.037.

[29] E. Jalali Dil, B.D. Favis, Localization of micro and nano- silica particles in a high interfacial tension poly(lactic acid)/low density polyethylene system, Polymer (Guildf) 77 (2015) 156–166, https://doi.org/10.1016/j.polymer.2015.08.063.

[30] E. Jalali Dil, M. Arjmand, Y. Li, U. Sundararaj, B.D. Favis, Assembling copper nanowires at the interface and in discrete phases in PLA-based polymer blends, Eur. Polym. J. 85 (2016) 187–197, https://doi.org/10.1016/j.eurpolymj.2016.09.053.

[31] T. Parpaite, B. Otazaghine, A.S. Caro-Bretelle, A. Taguet, R. Sonnier, J.M. Lopez-Cuesta, Janus hybrid silica/polymer nanoparticles as effective compatibilizing agents for polystyrene/polyamide-6 melted blends, Polymer (Guildf) 90 (2016) 34–44, https://doi.org/10.1016/j.polymer.2016.02.044.

[32] S. Weiss, D. Hirsemann, B. Biersack, M. Ziadeh, A.H.E. Müller, J. Breu, Hybrid Janus particles based on polymer-modified kaolinite, Polymer (Guildf) 54 (2013) 1388–1396, https://doi.org/10.1016/j.polymer.2012.12.041.

[33] X. Yan, A. Cayla, E. Devaux, B. Otazaghine, F. Salaün, Polypropylene/Poly(vinyl alcohol) blends compatibilized with kaolinite Janus hybrid particles and their transformation into fibers, Ind. Eng. Chem. Res. 58 (2019) 10931–10940, https://doi.org/10.1021/acs.iecr.9b01990.

[34] M. Batistella, B. Otazaghine, R. Sonnier, A.-S. Caro-Bretelle, C. Petter, J.-M. Lopez-Cuesta, Fire retardancy of ethylene vinyl acetate/ultrafine kaolinite composites, Polym. Degrad. Stabil. 100 (2014) 54–62, https://doi.org/10.1016/j.polymdegradstab.2013.12.026.

[35] M. Sahnoune, A. Taguet, B. Otazaghine, M. Kaci, J.-M. Lopez-Cuesta, Inner surface modification of halloysite nanotubes and its influence on morphology and thermal properties of polystyrene/polyamide-11 blends, Polym. Int. 66 (2017) 300–312, https://doi.org/10.1002/pi.5266.

[36] M. Sahnoune, A. Taguet, B. Otazaghine, M. Kaci, J.-M.J.-M. Lopez-Cuesta, Effects of functionalized halloysite on morphology and properties of polyamide-11/SEBS-g-MA blends, Eur. Polym. J. 11 (2017) 1–27, https://doi.org/10.1016/j.eurpolymj.2017.03.008.

[37] Y. Lvov, E. Abdullayev, Functional polymer–clay nanotube composites with sustained release of chemical agents, Prog. Polym. Sci. 38 (2013) 1690–1719, https://doi.org/10.1016/j.progpolymsci.2013.05.009.

[38] J.A. Galloway, C.W. Macosko, Comparison of methods for the detection of cocontinuity in poly(ethylene oxide)/polystyrene blends, Polym. Eng. Sci. 44 (2004) 714–727, https://doi.org/10.1002/pen.20064.

[39] J. Plattier, L. Benyahia, M. Dorget, F. Niepceron, J.-F. Tassin, Viscosity-induced filler localisation in immiscible polymer blends, Polymer (Guildf) 59 (2015) 260–269, https://doi.org/10.1016/j.polymer.2014.12.044.

[40] E. Chibowski, Determination of surface free energy of kaolinite, Clay Clay Miner. 36 (1988) 455–461, https://doi.org/10.1346/CCMN.1988.0360511.

[41] A. Göldel, G. Kasaliwal, P. Pötschke, Selective localization and migration of multiwalled carbon nanotubes in blends of polycarbonate and poly(styrene-acrylonitrile), Macromol. Rapid Commun. 30 (2009) 423–429, https://doi.org/10.1002/marc.200800549.

[42] A. Göldel, A. Marmur, G.R. Kasaliwal, P. Pötschke, G. Heinrich, Shape-dependent localization of carbon nanotubes and carbon black in an immiscible polymer blend during melt mixing, Macromolecules 44 (2011) 6094–6102, https://doi.org/10.1021/ma200793a.

[43] R. Krishnamoorti, R.A. Vaia, E.P. Giannelis, Structure and dynamics of polymer-layered silicate nanocomposites, Chem. Mater. 4756 (1996) 1728–1734.

[44] L. Elias, F. Fenouillot, J.C. Majeste, P. Cassagnau, Morphology and rheology of immiscible polymer blends filled with silica nanoparticles, Polymer (Guildf) 48 (2007) 6029–6040, https://doi.org/10.1016/j.polymer.2007.07.061.

[45] X.-Q. Liu, Q.-Y. Wang, R.-Y. Bao, W. Yang, B.-H. Xie, M.-B. Yang, Suppressing phase retraction and coalescence of co-continuous polymer blends: effect of nanoparticles

and particle network, RSC Adv. 4 (2014) 49429–49441, https://doi.org/10.1039/C4RA09138H.

[46] M. Sumita, K. Sakata, S. Asai, K. Miyasaka, H. Nakagawa, Dispersion of fillers and the electrical conductivity of polymer blends filled with carbon black, Polym. Bull. 25 (1991) 265–271.

[47] F. Gubbels, S. Blacher, E. Vanlathem, R. Jérôme, R. Deltour, F. Brouers, P. Teyssié, Design of electrical conductive composites: key role of the morphology on the electrical properties of carbon black filled polymer blends, Macromolecules 28 (1995) 1559–1566, https://doi.org/10.1021/ma00109a030.

[48] F. Gubbels, R. Jerome, E. Vanlathem, R. Deltour, S. Blacher, F. Brouers, Kinetic and thermodynamic control of the selective localization of carbon black at the interface of immiscible polymer blends, Chem. Mater. 10 (1998) 1227–1235, https://doi.org/10.1021/cm970594d.

[49] M. Trifkovic, A.T. Hedegaard, M. Sheikhzadeh, S. Huang, C.W. Macosko, Stabilization of PE/PEO cocontinuous blends by interfacial nanoclays, Macromolecules 48 (2015) 4631–4644, https://doi.org/10.1021/acs.macromol.5b00354.

[50] H. Xiu, Y. Zhou, C. Huang, H. Bai, Q. Zhang, Q. Fu, Deep insight into the key role of carbon black self-networking in the formation of co-continuous-like morphology in polylactide/poly(ether)urethane blends, Polymer (Guildf) 82 (2016) 11–21, https://doi.org/10.1016/j.polymer.2015.10.034.

[51] A.L. Persson, H. Bertilsson, Viscosity difference as distributing factor in selective absorption of aluminium borate whiskers in immiscible polymer blends, Polymer (Guildf) 39 (1998) 5633–5642, https://doi.org/10.1016/S0032-3861(98)00096-2.

[52] A. Taghizadeh, B.D. Favis, Carbon nanotubes in blends of polycaprolactone/thermoplastic starch, Carbohydr. Polym. 98 (2013) 189–198, https://doi.org/10.1016/j.carbpol.2013.05.024.

[53] M. Huang, Z. Li, H. Guo, The effect of Janus nanospheres on the phase separation of immiscible polymer blends via dissipative particle dynamics simulations, Soft Matter 8 (2012) 6834, https://doi.org/10.1039/c2sm25086a.

[54] A. Walther, K. Matussek, A.H.E. Müller, Engineering nanostructured polymer blends with controlled nanoparticle location using Janus particles, ACS Nano 2 (2008) 1167–1178, https://doi.org/10.1021/nn800108y.

[55] H. Wang, X. Yang, Z. Fu, X. Zhao, Y. Li, J. Li, Rheology of nanosilica-compatibilized immiscible polymer blends: formation of a "heterogeneous network" facilitated by interfacially anchored hybrid nanosilica, Macromolecules 50 (2017) 9494–9506, https://doi.org/10.1021/acs.macromol.7b02143.

[56] S.S. Ray, R. Salehiyan, Chapter 7: effect of mixing conditions (dynamic process), in: Nanostructured Immiscible Polymer Blends, Elsevier, 2020, pp. 107–142.

[57] N.O. Jaensson, C. Mitrias, M.A. Hulsen, P.D. Anderson, Shear-induced migration of rigid particles near an interface between a Newtonian and a viscoelastic fluid, Langmuir 34 (2018) 1795–1806, https://doi.org/10.1021/acs.langmuir.7b03482.